Hydrological classification by clustering approach of time-integrated samples at the outlet of the Rhône River: application to Δ14C-POC

Nathan Bodereau, Adrien Delaval, Hugo Lepage, Frederique Eyrolle, Patrick Raimbault, Yoann Copard

Hydrological classification by clustering approach of time-integrated samples at the outlet of the Rhône River: application to Δ^{14}C-POC

Nathan Bodereau[1*], Adrien Delaval[1,2], Hugo Lepage[1], Frederique Eyrolle[1], Patrick Raimbault[3], Yoann Copard[4]

[1] *Institute for Radioprotection and Nuclear Safety (IRSN), PSE-ENV/LRTA, PSE-ENV/LMRE, BP 3, 13 115, Saint-Paul-lez-Durance, France*

[2] *Adict Solutions, Campus INP ENSAT, Avenue de l'Agrobiopole, BP 32 0607, 31 326 Castanet-Tolosan, France*

[3] *Aix Marseille Université, CNRS/INSU, Université de Toulon, IRD, Mediterranean Institute of Oceanography (MIO) UM 110, 13288, Marseille, France*

[4] *Normandie Univ, UNIROUEN, UNICAEN, CNRS, M2C, France, 76000 Rouen, France*

** Corresponding author.*

E-mail address: bodereau.nathan@gmail.com

Highlights

- *The classification of the Rhône River hydrology was obtained by fuzzy C-mean logic*
- *A 5-Cluster configuration is efficient to characterize Rhône River hydrology*
- *Δ^{14}C-POC distribution among each cluster confirms the main assessments in literature*
- *This approach allows to identify the contribution of each hydrology to samples*

Abstract

Within the framework of the Rhône Sediment Observatory, monthly time-integrated samples have been collected by Particle Traps in the last decade to monitor particulate contaminants in the Rhône River and its main tributaries. In this watershed with a contrasted hydrology, a clustering approach is used to classify the samples according to the main hydrological events. This approach has been applied to riverine particulate organic radiocarbon signatures (Δ^{14}C-POC) that are strongly affected by the origin of the material and the occurrence of nuclear power plant releases. Suspended Particulate Matter (SPM) samples were collected near the outlet of the Rhône River and analysed for ^{14}C along with particulate organic carbon (POC), chlorophyll a and tritium contents to confirm Δ^{14}C-POC origins. Cluster Analysis, coupled to Principal Component Analysis, were performed based on monthly average water discharges of the Upper Rhône River and the five main tributaries. The classification obtained by fuzzy C-mean logic of the Rhône River hydrology into 5 clusters is similar to that already observed in the literature with Mediterranean/Cevenol flood, oceanic pluvial flood, nival flood, low-water level and baseflow clusters. The contribution of each cluster among the Δ^{14}C-POC values demonstrate the complexity of hydrological classification of time-integrated samples. First, the samples with a unique and significantly dominant cluster are easily explained with negative Δ^{14}C-POC values observed in the flood clusters due to input of ^{14}C-depleted material from soil or rock weathering, and positive values observed in the low-water level and baseflow clusters due to anthropogenic input by nuclear industry. Second, samples that present a homogeneous mixture between several clusters demonstrate the occurrence of different hydrological events during the sampling periods. This tool appears as a solution to estimate the contribution of each hydrological event classification in time-integrated samples.

Keywords : Hydrological distribution, Cluster Analysis, Radiocarbon, Particulate Organic Carbon.

1. Introduction

Rivers are unquestionably links between the Earth system reservoirs as they connect 87 % of the Earthland surface to the oceans (Meybeck, 1982). They are also the receptacle of pollutants such as organic and inorganic micropollutants due to agricultural, industrial, domestical and mining activities (Meybeck, 2003) but also artificial radionuclides that are released by nuclear industries (Eyrolle et al., 2020).

Suspended Particulate Matter (SPM) is one of the aquatic fractions and belongs to sedimentary systems with processes of particles burying and remobilisation within river systems entering in the long-term cycle (Leithold et al., 2016). Photosynthesis, microbial oxidation, floodplain sediment remobilisation, sediment introduction are so many processes that can affect pollutant composition across the river (Meybeck et al., 2003; Walling et al., 2003). Thus, monitoring riverine SPM dynamic is of a great challenge in the perspective of health risk assessment, ecological restauration or river management (Walling et al., 2003). The development of network monitoring of SPM and pollutant fluxes has been performed over these last decades using SPM discrete sampling (Horowitz et al., 2001) but their frequencies of acquisition are still be constrained to event with a fixed periodicity, such as flood, and variations of SPM concentration (C_{SPM}) that can occur between samples are often omitted (Misset et al., 2019) .

The deployment of Particle Traps (PT) has been described as a serious alternative from direct sample as they are time-integrative, low cost and easily handled (Phillips et al., 2000; Schulze et al., 2007). However, they can cover periods that might integrate several hydrological

events and affect our knowledge on contaminant dynamic (Poulier et al., 2019). Thus, constraining hydrosedimentary behaviours of river systems using time-integrated sample is challenging. Multivariate analysis and clustering to characterize catchment seasonal hydrology could be linked with time-integrated sample. The Principal Component Analysis (PCA) coupled to Clustering Analysis (CA) has been widely used in Earth and Environmental sciences (e.g., Delaval et al., 2021, Raux et al., 2011). It is also an usual method for data mining when it comes to identify groups and classify individuals. However, many algorithms exist and present different results and convergence speeds (Jain et al., 1999). Fuzzy c-mean algorithms are usually considered as reliable algorithms in environmental sciences (Delaval et al., 2021, Kim et al., 2011). Their success is due to their simple geometric criteria and their robustness without any prior information on the cluster structure such as possible overlap or sphericity (Kamel and Selim, 1994). In addition, the fuzzy approach provides cluster membership degrees (probability for an observation to belong to a cluster) instead of sharp cluster boundaries. As a result, the ambiguity of the data can be preserved and these probabilities can be used later for post treatments or deeper interpretations (Kim et al., 2011).

The Rhône River is one of the major sources of freshwater and SPM to the Mediterranean Sea (Milliman and Farnsworth, 2011). It is also a strongly anthropized catchment where inorganic and organic pollutants are monitored for several decades (e.g., Delile et al., 2020; Eyrolle et al., 2018; Launay et al., 2019; Ollivier et al., 2011; Poulier et al., 2019; Radakovitch et al., 2008). Within the Rhône Sediment Observatory (OSR) framework, SPM are collected every month on the Rhône River and its main tributaries using PT (Lepage et al., 2022). While the results demonstrate a strong link between the contaminant concentrations and the hydroclimatic heterogeneities of this catchment including different tributary regimes (e.g.,

92 Delile et al., 2020; Poulier et al., 2019), the occurrence of different events in a same time-
93 integrated sample may lead to a bias in interpretation.
94 In this study, we propose to classify time-integrated samples according to hydrological
95 events using a clustering approach and to investigate the distribution of the clusters among
96 the concentrations of $\Delta^{14}C$ (Carbon 14 reported to 1950 standard) in Particulate Organic
97 Carbon (POC). Here, the challenge is that while the hydrology of the Rhône River was already
98 classified based on hourly or daily water discharge values by previous studies (e.g., Mourier
99 et al., 2014; Ollivier et al., 2011; Poulier et al., 2019; Radakovitch et al., 2008; Zebracki et al.,
100 2015), time-integrated samples, that can cover periods from two weeks to one month, might
101 integrate several hydrological events (Delile et al., 2020; Poulier et al., 2019). The hydrology
102 of the Rhône River main tributaries during time-integrated sampling (164 samples) has been
103 classified with a fuzzy-C mean algorithm. Carbon-14 (^{14}C), expressed as $\Delta^{14}C$, in riverine POC,
104 is a radioisotope occurring naturally in the upper parts of the atmosphere and from
105 anthropogenic sources such as atmospheric nuclear weapon tests (1945-1990) or releases of
106 nuclear industries (Eyrolle et al., 2018). The ^{14}C-POC is selected here because its dynamic in
107 the Rhône River is well documented: ^{14}C-labelled POC by nuclear industry releases during
108 low-water level is opposite to depleting ^{14}C-POC by introduction of ^{14}C-dead Carbon, during
109 floods, coming from rock or soil weathering (Copard et al., 2018 ; Eyrolle et al., 2018; in
110 review). Geochemical indicator distributions have been then discussed such as POC content
111 in SPM (%POC) and Chlorophyll a content in POC (%Chl.a) to study the distribution of the
112 clusters among the $\Delta^{14}C$-POC. To identify potential artificial ^{14}C releases, tritium
113 concentrations collected in water masses were also investigated.

2. Material and methods

2.1. Study area

The Rhône River basin covers a 98 500 km² area (**Figure 1**), with a river stream length of 816 km. The watershed boundaries are delimited with the presence of the Alps, Jura, Cevennes and Vosges mountains lidding to a string topographic gradient and hydroclimatic heterogeneities (Olivier et al., 2009). It encompasses tributaries with contrasted hydrologies :

i) oceanic pluvial regime observed at the North of the watershed in winter (Saône and Ain rivers);

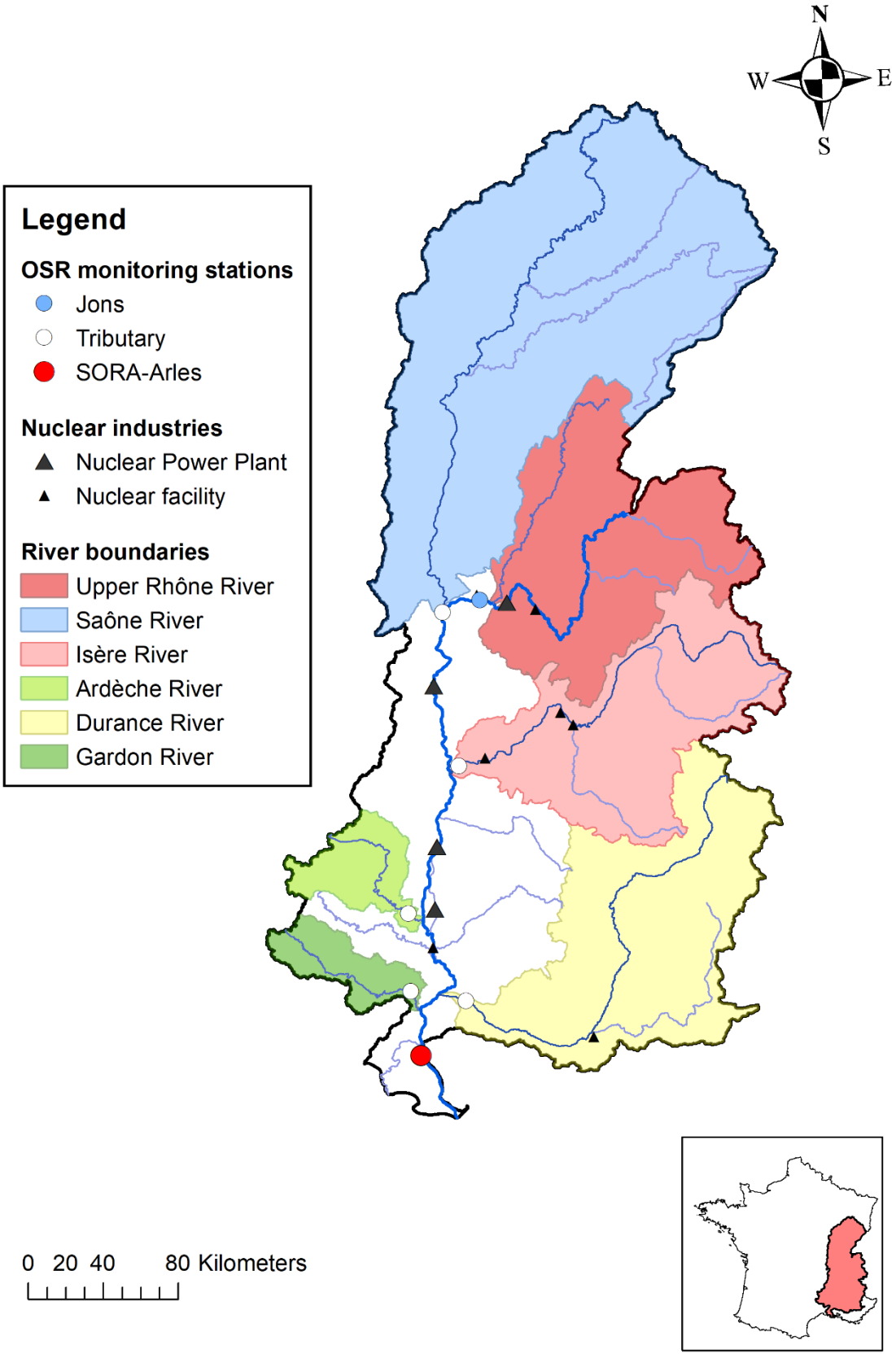

124

125 Figure 1 – Map of the Rhône watershed with the delimitations of main tributary basins discussed in this study.

126 The locations of SORA and Jons stations, the tributary stations and the nuclear industries are also added.

ii) flash Mediterranean rainfalls, coming from Mediterranean Sea, and generally observed in autumn, that occur in the Southeastern part of the watershed (Durance, Drôme and Ouvèze rivers);

iii) flash Cevenol rainfalls that conduct to the same sharp flow variation than Mediterranean floods but occur early in fall season and are more located around the Cevennes mountains (Ardèche, Cèze and Gardon rivers);

iv) alpine regimes linked to the snow melt and generally occurring in Alps tributaries (Arve, Fier, Isère and Durance rivers) during spring;

v) generalized floods that encompass all flood events (Delile et al., 2020, Pont et al., 2002, Sadaoui et al., 2016).

In addition, fourteen nuclear reactors and various nuclear industries are distributed along the Rhône River making it as one of the most nuclearized river in the world (Eyrolle et al., 2020).

2.2. Sampling methodology

Samples were collected at the SORA monitoring station that is located at the outlet of the Rhône River, 47 km upstream from the mouth, and has been designed to monitor river inputs into the Mediterranean Sea (Lepage et al., 2022). It is located on the "Grand Rhône" branches where 90% of the water and sediment fluxes of the Rhône River are transiting, while the remaining 10% transit through the "Petit Rhône" (Pont et al., 2002). Water intake is performed on a floatable structure at 7 m from the bank and 0.5 m under the surface

regardless the water discharge and continuously supplies the sampling devices (Lepage et al., 2022).

The SPM are collected over a two-week to one-month period in PT, designed with the same characteristics as described by Schulze et al. (2007), deep-frozen (-18°C), freeze-dried, and finally homogenized by grinding in an agate mortar. SPM samples are stored in the dark and at ambient temperature before analysis (Lepage et al., 2022). A total of 164 samples were collected at SORA from 2007 to 2020 and Δ^{14}C-POC was measured among 54 of them.

POC and Chlorophyll a are separately measured in SPM filtered in daily composite water samples. Sampling is achieved using a cooled automatic water sampler that fills a daily bottle with 150 mL every 90 minutes to constitute a composite sample each day (Eyrolle et al., 2020). The sampling frequency is reduced to every 30 minutes to constitute a composite sample every 4 hours when water discharge is greater than 3000 m^3 s^{-1}. Samples are poisoned with $HgCl_2$ and kept at 5°C until they are filtered on a 0.7 Whatman pre-conditioned glass fiber filters GF/F (dried at 500°C for 4 hours). The samples are then frozen, respectively, until laboratory analysis (Lepage et al., 2022). For tritium analysis, a few millimeters of water is collected per 80 minutes to obtain a monthly composite sample. Water is then filtered through 0.22 µm GF/F before analysis (Eyrolle et al., 2020).

2.3. Principal Component Analysis (PCA) and Cluster Analysis (CA)

2.3.1. Input data

With the perspective to trigger all hydrologic regimes occurring on the Rhône according to the literature, the water discharges (Q) of the five main tributaries (Saône, Isère, Ardèche, Durance and Gardon rivers) as well as the measures conducted at the Jons monitoring

station, considered as the reference station to evaluate water discharge from the Upper Rhône River, were used to define the clusters (**Figure 1**). For those stations, daily averaged water discharge data are continuously measured (Thollet et al., 2021) at the exception of the Upper Rhône station (Jons) where Q is estimated from a 1D hydrodynamic model with water discharges of upstream main tributaries as input data (Launay et al., 2019).

Mean water discharge values (Q_{mean}) for each tributary and Jons monitoring stations were estimated from the start to the end of each 164 PT samples and submitted in PCA. We assumed that this is enough to characterized tributary hydrograph shapes for each period of acquisition (Hannah et al., 2000, Ouyang et al., 2010).

In order to better interpret the results of the PCA and the clustering, hydrological data (Q and C_{SPM}) at the SORA station was also used so as the C_{SPM} of the tributary stations if available. At SORA, daily averaged water discharge data are continuously measured (Thollet et al., 2021) while the SPM concentration (C_{SPM}) at SORA station is measured by time-integrating weighing of daily automatic samples (AFNOR, 2005). At tributaries, averaged daily C_{SPM} is estimated from turbidity and C_{SPM} rating curves with 10-minute frequency of acquisition and monthly automatic water samples (Lepage et al., 2022). A mean value ($C_{SPM-mean}$) was calculated for each PT sample.

2.3.2. PCA and CA algorithms

The PCA has been performed using R programming language including the R packages "FactoMineR" for PCA (Husson et al., 2010), "e1071" (Meyer et al., 2021) and "fclust" for fuzzy c-mean algorithms (Ferraro et al., 2019). The goal of PCA is to describe a data set using a smaller number of uncorrelated variables, while retaining as much information (variance) as possible. The reduction is achieved by transforming the data into a new set of continuous

variables named the principal components. The reduction of dimensionality provides a framework to visualize the Rhône hydrology. The essential of the information being on the first components (Husson et al., 2010), PCA is usually used as a pre-processing tool before clustering analysis (Delaval et al., 2021).

Then, clustering algorithms such as c-mean algorithms (crisp or fuzzy) classify individuals according to their variable similarities and allows to identify scenarios and trends in river hydrology and hydrochemistry. This is done by randomly defining i centroids in the same coordinate systems as the individuals. Each individual x (total of k) is assigned to the closest centroid center C_i. The barycenter of each subgroup is then calculated and becomes the new centroid. This procedure converges when the centroids are no longer moving. In addition, the fuzzy alternative introduces two new parameters. The first one is the membership coefficient. This membership represents how closely the k_{th} data object (x_k) is located from the i_{th} Cluster center. Membership score indicates the degree (in %) to which a sample belongs to each cluster. Each sample is assigned to the cluster with the highest membership among the others.

The second parameter m is the fuzzifier. It is greater than 1 and usually dependent on the dataset structure because it represents the degree of overlap of the clusters (Klawonn and Höppner, 2003). When m is close to one, the solution of the fuzzy c-means algorithm is similar to the one of c-means. Elements are simply assigned to only the nearest cluster and membership to other clusters is nearly existent. When m is large, fuzziness is also large and clusters are blurred which can be a more accurate description of the system. More details about c-mean algorithms are provided in Bezdek et al., (1988).

The best combination of {*C*, *m*} parameters is not determined by the algorithm. One approach is to run different simulations with different {*C*,*m*} pairs and to check the efficiency of clustering with a quality criteria (Ramze Rezaee et al., 1998). River hydrology related to clustering studies have a number of clusters falling in the interval [2,8] (Delaval et al., 2021; Javed et al., 2021; Ouyang et al., 2010). Our number of Δ^{14}C-POC observations being limited (n=54), we are expecting 8 clusters at most (Chaimontree et al., 2010) and we will set the test interval for the number of clusters to [2,8].

The fuzzifier *m* can be in theory any real number between 1 and ∞. *m* is usually set to 2 by default but can be any real number between 1 and ∞ usually decreasing with dataset size (Klawonn and Höppner, 2003). In our tests, we will take 1 as the lower limit for *m*. The upper limit is *m*=3 according to the empirical threshold equation based on the length and dimensions of the dataset proposed by Schwämmle and Jensen (2010). As a result, we will perform clustering on the interval [2,8] for C, the number of clusters and on the interval]1,3] for *m* the fuzzifier.

2.4. Analyses

2.4.1. Carbon-14 measurement

The ^{14}C measurement in SPM are performed using a 3 MV NEC PELLOTRON Accelerator Mass Spectrometry (Artemis AMS facility, Dumoulin et al., 2017). Briefly, SPM samples are firstly decarbonated with 0.5 M HCl, placed in Pyrex sealed tubes and calcined (850°C for 5 hours). CO_2 is collected into a glass line under vacuum (< 10^{-5} mbar) and cryogenically trapped via liquid nitrogen. The sample CO_2 is reduced with hydrogen and iron powder as a catalyser following the protocol of Voegel et al., (1984) and pressed into an aluminium cathode (1 mm hole diameter) to form a graphite target.

In the AMS, the target is submitted to high bombing with Caesium sputter ion sources and sequentially sent, through a 90° magnet, to an accelerator tube. Here, Carbon isotopes are stripped in an argon gas and distinguished through a 45° analyser according to their weight. ^{14}C ions are counted in an ionization chambers (Cottereau et al., 2007).

After AMS counting, the $^{14}C/^{12}C$ ratio R is normalized (R_n) to a $\delta^{13}C$ of –25‰ in order to take into account carbon isotopic fractionation (Stuiver and Polach, 1977) . A 1950 standard R_s (i.e., oxalic acid II, a crop of sugar beet) is also incorporated in the sample batch and normalized as R_{sn}. Following Stuiver and Polach (1977) formulation, $\Delta^{14}C$ is privileged in order to take into account radiodecay (**Equation 1**) with *y*, the year of measurement and the Godwin's mean life (8267) estimated from soil and water samples (Godwin et al., 1962).

$$\Delta^{14}C = \left(\frac{R_n}{R_{sn}} \times e^{\left(\frac{y-1950}{8267}\right)} - 1\right) \times 1\,000 \qquad \textit{Equation 1}$$

Carbon, after the 1950 standard, has a $\Delta^{14}C$ up to 0 ‰ and could integrate the contribution of anthropogenic sources such as the effects of thermonuclear weapon tests (1945-1990) or releases of nuclear industries. Values reaching -1000‰ are linked to material old of up 50 000 years BP (Trumbore et al., 2016).

2.4.2. Particulate nutrient and tritium analyses

The POC concentration measurements were carried out at the Mediterranean Institute of Oceanography (M.I.O.) and were performed on daily decarbonated SPM by using high combustion procedure (950°C) on a Carbon Nitrogen (CN) Integra mass spectrometer (serCon Ltd, Crewe, UK) as described in Raimbault et al. (2008). Chlorophyll a measurement is conducted through fluorimetry methodology after its extraction with methanol according

to Raimbault et al. (2004). Tritium analyses (Bq l^{-1}) were carried out at the LMRE/IRSN by liquid scintillation counting (AFNOR, 2015).

3. Results

3.1. Data description

The distributions of environmental data treated by CA are available in *Dataset S1*. The Q_{mean} and $C_{SPM\text{-}mean}$ histories are respectively presented in **Figures 2.a.** and **2.b**. and Δ^{14}C-POC values in **Figure 2.c.**

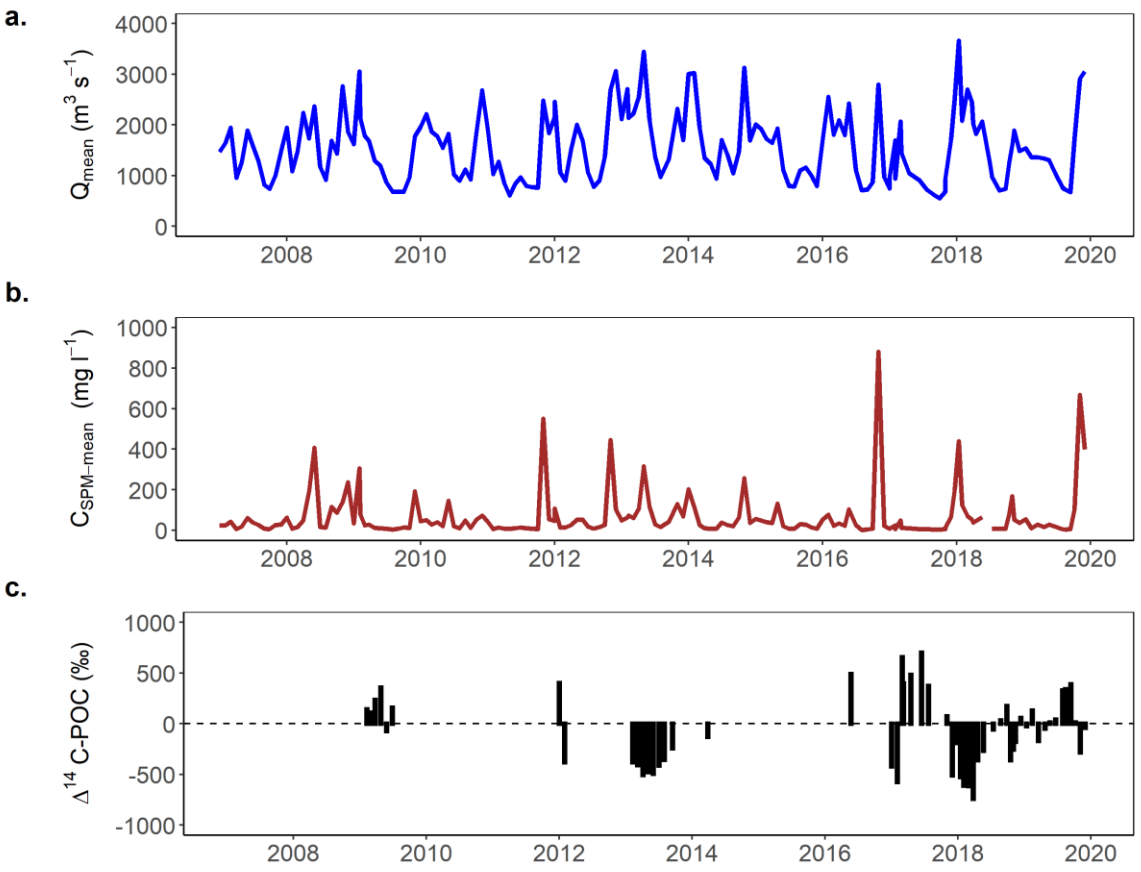

Figure 2 - Distribution of a.) Q_{mean} (n = 164), b.) $C_{SPM\text{-}mean}$ (n = 163) and c.) Δ^{14}C-POC values (n = 54) over the 2007-2020 period.

During the whole 2007-2020 period, for all 164 samples, $Q_{mean,}$ at Arles varied between 558 and 3 668 $m^3 s^{-1}$ (mean= 1 565 $m^3 s^{-1}$, s.d. = 687 $m^3 s^{-1}$) while $C_{SPM\text{-}mean}$ varied between 2.9 mg l^{-1} and 879.7 mg l^{-1} (mean= 68.3 mg l^{-1}, s.d. = 117.4 mg l^{-1}). Δ^{14}C-POC signatures are ranged from -742 to 699 ‰ (mean = -84.5 ‰, s.d. = 346 ‰). The signatures are unequally distributed over the period (**Figure 2.c.**) because Δ^{14}C-POC analyses in SPM have been continuously performed since 2014 despite some exceptional measurements performed around 2009 and 2012 (Eyrolle et al., 2018).

The average POC content in SPM (%POC) is estimated between 1.03% and 10.37% (mean= 3.95 %, s.d. = 1.73 %). The average chlorophyll a content in POC (%Chl.a) is varying between 0.01% and 2.15 % (mean = 0.34 %, s.d. = 0.42 %), while tritium concentrations in water between 0.4 and 20.7 Bq l^{-1} (mean = 6.1 Bq l^{-1}).

3.2. Principal Component Analysis

The PCA transformed the variables (mean Q for the five tributaries and Jons) into six vectors (**Figures 3a and b**).

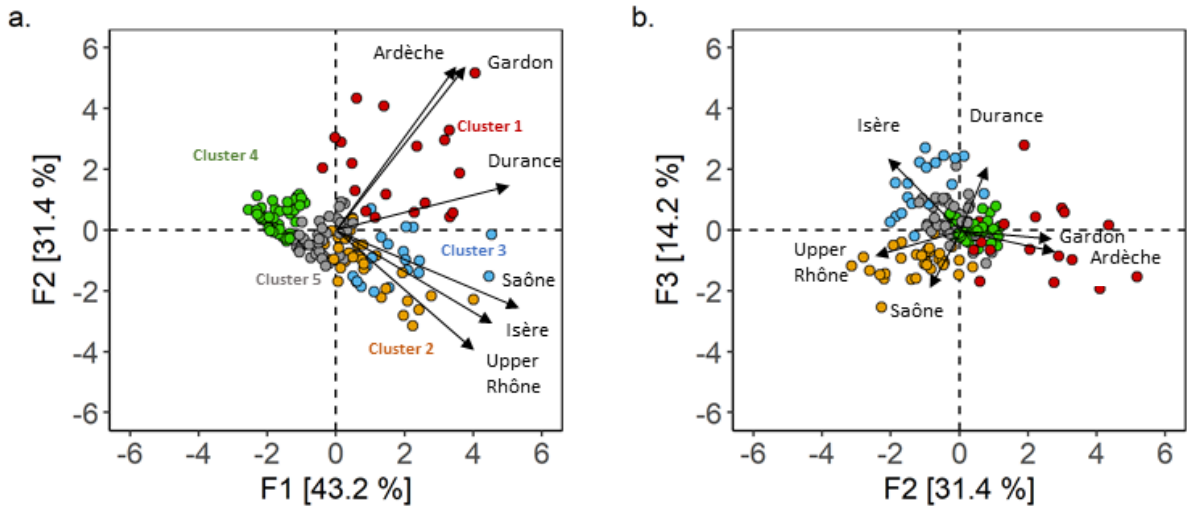

Figure 3 – Principal component analyses 1 and 2 of the dataset. The PCA were conducted on the mean of the water discharge of the five main tributaries of the Rhône River (Saône, Isère, Ardèche, Gardon and Durance rivers) and the station of Jons that monitors the Upper Rhône River. Clusters are highlighted by colours.

The F1 axis explains 43.2 % of the variance of the dataset and all tributary vectors are oriented toward the right side of the PCA. The F2 axis, explaining 31.4% of the variance, distinguishes, from the top to the bottom, southern tributaries (Ardèche, Gardon and Durance rivers) and northern ones (Saône, Isère and Upper Rhône rivers) (**Figure 3.a**.). Through the F1 × F2 axis configuration (PCA1), the observations are concentrated around the 0 axis on the left side of F2 while they are scattered on the right side. Through the F2 × F3 axis (14.2% of the variance) configuration (PCA2), the Isère and Durance vectors are located on the top side of the PCA whereas other vectors are located on the bottom side. As observed for PCA1, Ardèche and Gardon vectors are grouped. The F4 axis explains 6.6 % of the variability and separates Durance and Saône rivers from other tributaries (*Suplementary information, Figure S1*). Through F3 × F4 axis configuration (PCA3), samples are centred and staggered across the F4 axis.

3.3. Cluster number assessment

The fuzzy clustering was performed with the first four components of the PCA in order to cumulate an explained variance of up to 95 % (*Figure S2*). The performances were estimated through Xie and Beni index (XB) (to minimize) according to different {C,m} simulations (*Table S1*)**.** The five-cluster configuration showed the lowest score (m = 13, XB = 0.296) and will be retained for the remainder of this work.

3.4. Hydrodynamic distribution for each cluster

Respectively, 12.1 %, 20.1 %, 11.6 %, 31.2 % and 25.0 % of Q_{mean} are distributed among clusters 1, 2, 3, 4 and 5. The Q_{mean} and $C_{SPM\text{-}mean}$ distributions at Arles, Jons and tributaries are respectively available in *Tables S2 and S3*. In both PCA1 and PCA2, Cluster 1 includes Ardèche and Gardon vectors (**Figures 3a and 3b**). For clusters 2 and 3, the results are contrasted. In PCA1, Cluster 2 integrates the three northern stations while in PCA2 the Isère vector is excluded. For Cluster 3, only the Isère vector is included in PCA2 while the Saône vector is included in PCA1. Finally, in both configurations, the Durance vector is located between clusters 1 and 3.

Clusters 1, 2 and 3 are characterized by a maximum Q_{mean} above the daily flood threshold at Arles (3000 $m^3\ s^{-1}$) with high standard deviations (up to 400 $m^3\ s^{-1}$). For clusters 1 and 3, similar results were observed for the $C_{SPM\text{-}mean}$ with average concentrations close to 200 mg l^{-1} at Arles and high values in the Ardèche (mean $C_{SPM\text{-}mean}$ = 27 mg l^{-1}), Durance (mean $C_{SPM\text{-}mean}$ = 661 mg l^{-1}) and Gardon (mean $C_{SPM\text{-}mean}$ = 58 mg l^{-1}) rivers for Cluster 1 and Isère (mean $C_{SPM\text{-}mean}$ = 333 mg l^{-1}) and Durance (mean $C_{SPM\text{-}mean}$ = 498 mg l^{-1}) rivers for Cluster 3. For

330 Cluster 2, while the $C_{SPM\text{-}mean}$ observed at Arles (mean $C_{SPM\text{-}mean}$ = 77 mg l^{-1}) are lower than
331 clusters 1 and 3 (mean $C_{SPM\text{-}mean}$ > 150 mg l^{-1}).

332 Located on the left side of the PCA1, Cluster 4 presents lowest values of Q_{mean} with a mean
333 at Arles of 849 $m^3.s^{-1}$. Cluster 4 is also characterized by the lowest $C_{SPM\text{-}mean}$ at Arles and for
334 all tributaries. Cluster 5 is centred between F1 and F2 with a predominance of the Isère and
335 Durance rivers (**Figure 3b**) and also of the Saône River but their discharges remain lower
336 than those observed in clusters 2 and 3. Cluster 5 presents moderate $C_{SPM\text{-}mean}$ at Arles
337 (mean= 33 mg l^{-1}) with low variability and moderate increases of the Durance and Isère
338 rivers $C_{SPM\text{-}mean}$ (77 and 54 mg l^{-1} respectively).

339 Percentages of occurrence for calendar months are presented in **Figure 4**. The samples for
340 Cluster 1 are generally centred in from October to December (maximum of 47%), February
341 (25%) and March (23%). Cluster 2 samples are mainly centred from December to April
342 (maximum of 67%). Cluster 3 is mainly observed from April to June (up to 46%). Cluster 4
343 samples are generally observed from July to November (up to 85%). Finally, Cluster 5 mainly
344 occurs from March to August with a peak in July (58%).

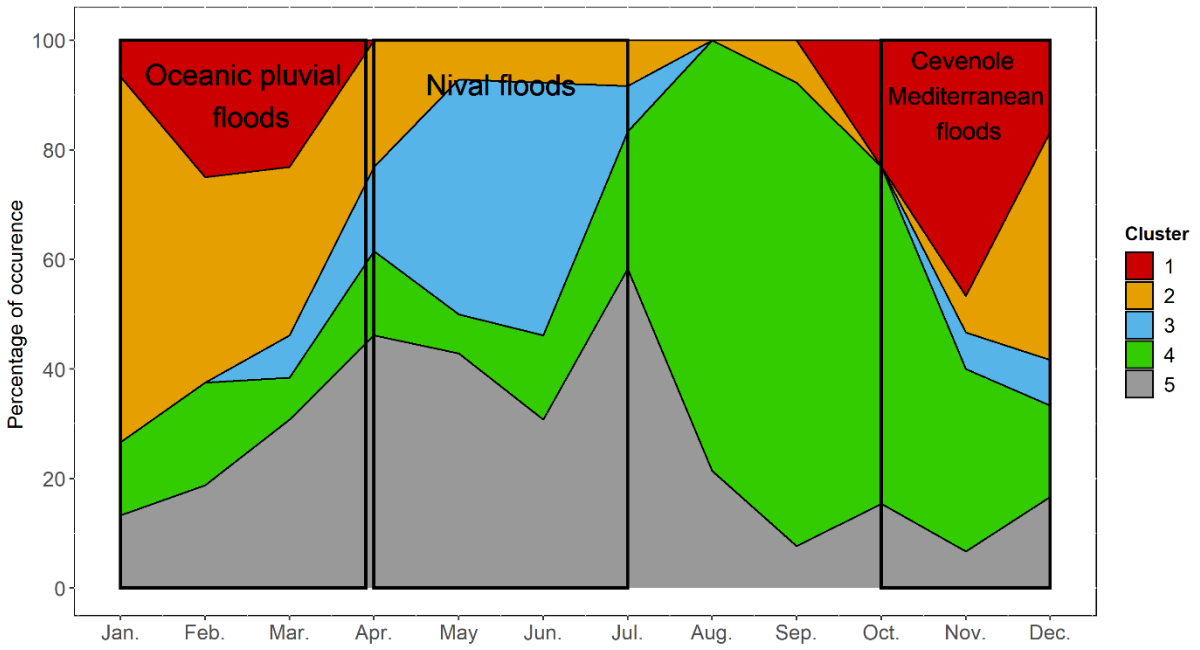

345 Figure 4 – Inter-annual occurrences of each cluster among the 164 samples. Flood delimitations were estimated from Delile
346 et al., 2020.

347

348 ## 3.5. Δ^{14}C-POC distribution among the clusters

349 Distribution of Δ^{14}C-POC among the clusters are presented in **Figure 5** where each value was
350 associated to the cluster with the highest contribution (**Figure 6**). While Δ^{14}C-POC values
351 cover all hydrological events, the number of Δ^{14}C-POC data is unequally distributed among
352 clusters (7, 7, 8, 12 and 20 respectively).

353

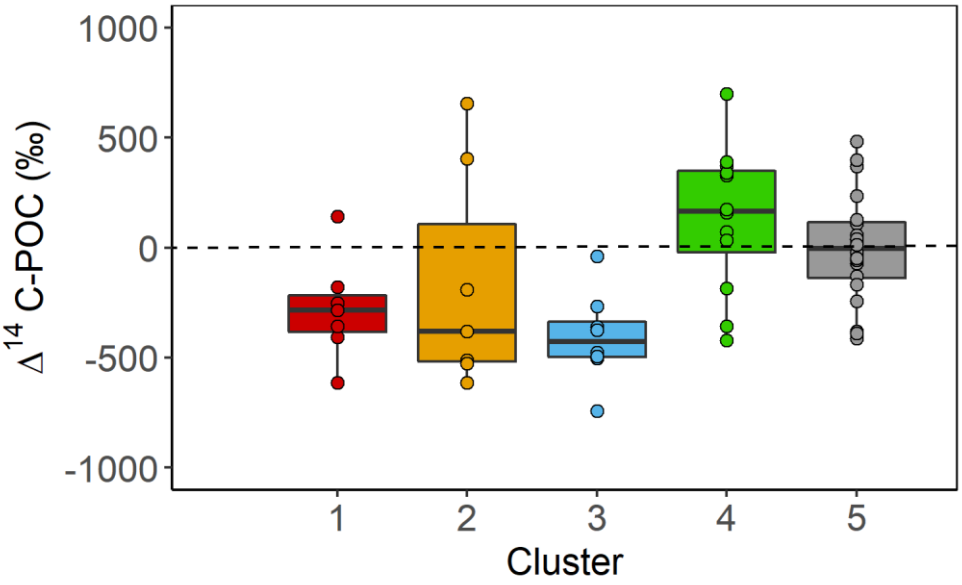

354

355 Figure 5 – Δ^{14}C-POC (n=54) distribution among the 5 clusters over the 2007-2020 period. Each value was associated to the
356 cluster with the highest membership score. Dotted horizontal line represents the year 1950 for which the value is 0 ‰ (cf.
357 **equation 1).**

358

359

360 Cluster 1, Cluster 2 and Cluster 3 include the lowest values with a median of -223, -367 and -
361 487‰. Cluster 2 includes the largest distribution of Δ^{14}C-POC signatures from - 613 to 655 ‰
362 while clusters 1 and 3 are concentrated between -614 and 142 ‰ and -742 and -40‰. Most
363 of the values of the Cluster 4 are above 0‰ with a median of 174 ‰, excepted for three
364 negative values (-420, -354 and -185 ‰). The Cluster 5 is equally centred around 0‰ with a
365 median of -24 ‰.

366 The dominant or attributed cluster in each sample is characterized by its membership degree
367 ranging from 25.8% to 84.6% (**Figure 6**). A few samples show a homogeneous cluster
368 membership score distribution highlighting that they could belong to another cluster than
369 the attributed one. For example, the sample with the highest Δ^{14}C-POC in Cluster 3 (-40‰)
370 presents membership degrees ranging from 13.3 to 26.7 %. Respectively 29%, 57%, 25%,

371 75% and 35% of the samples have an appurtenance degree to their attributed cluster higher

372 than 50% in Cluster 1 to 5.

373

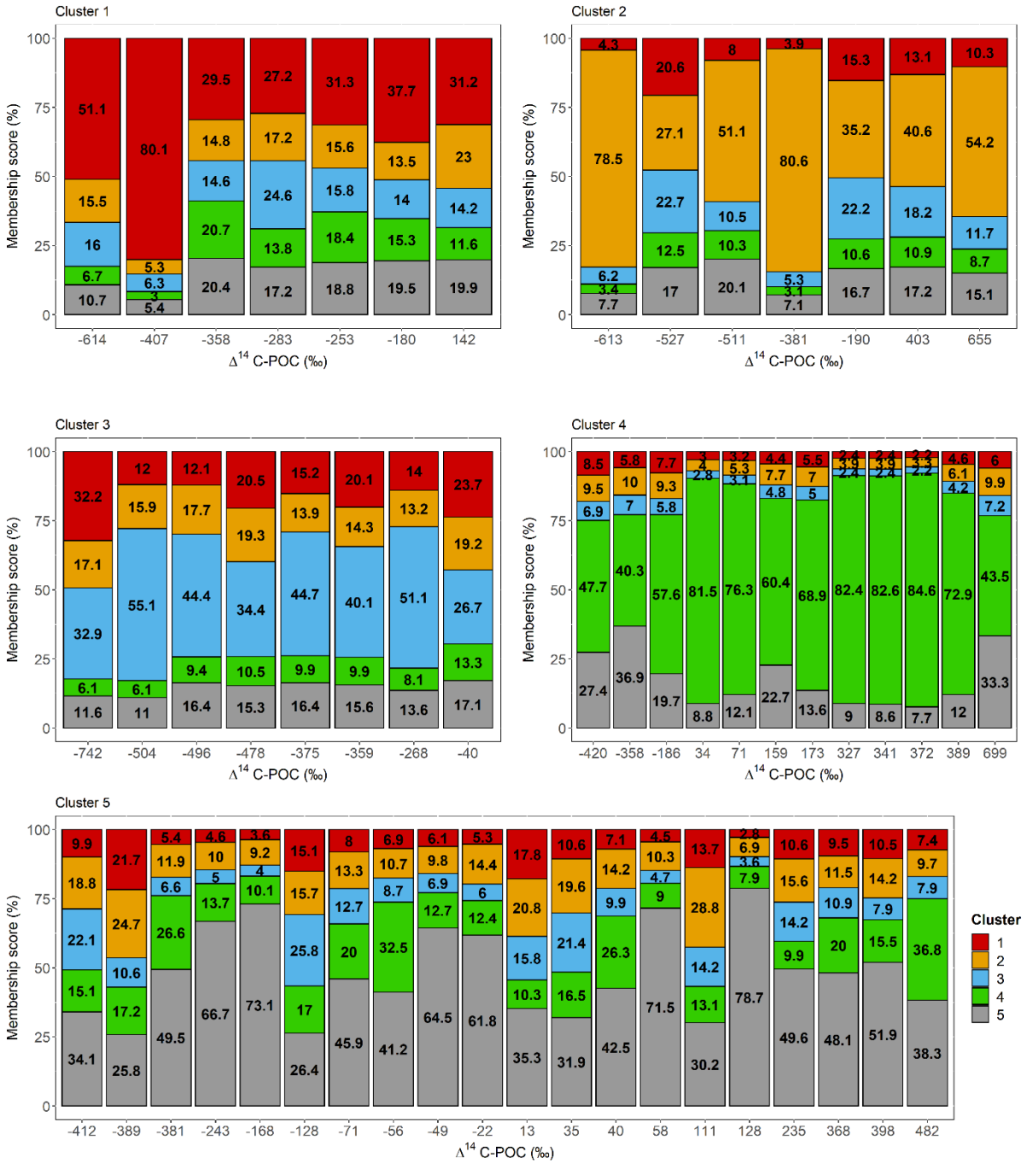

374

375 Figure 6 – Distribution of cluster memberships for Δ^{14}C-POC values (n = 54) among the classification. Each

376 membership score is expressed in %.

3.6. Geochemistry distribution

The Δ^{14}C-POC relationships with $C_{SPM\text{-}mean}$, average %POC, %Chl.a and tritium concentrations, among the 5 clusters, are presented in **Figure 7** . Overall, Δ^{14}C-POC shows positive relationships with %POC and a negative relationship with $C_{SPM\text{-}mean}$. High Δ^{14}C-POC are correlated with high %Chl.a (up to 0.6 %) and high tritium concentrations (up to 5 Bq l^{-1}). Cluster 1, 2 and 3 gather low %POC while clusters 4 and 5 present higher and more variable records. Highest %POC, %Chl.a. and tritium records are observed for Cluster 4 and Cluster 5 and some exceptions in Cluster 2.

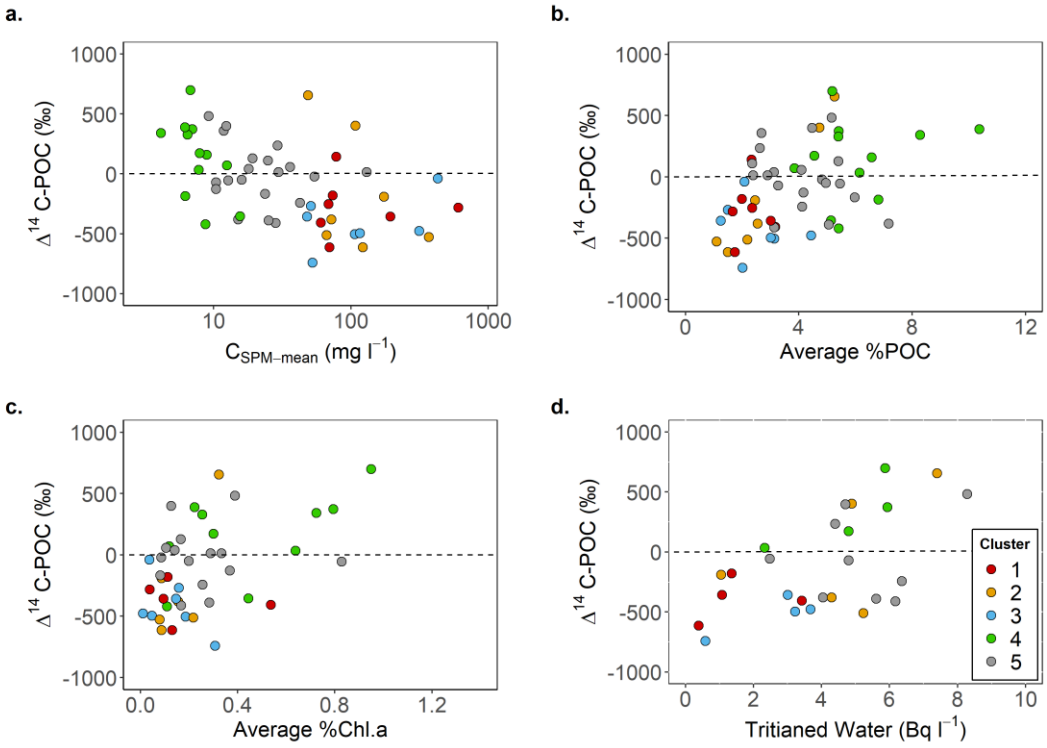

Figure 7 – Δ^{14}C-POC relationships with a.) $C_{SPM\text{-}mean}$, b.) average %POC, c.) average %Chl.a. and d.) tritium concentrations according to the cluster.

4. Discussion

4.1. Characterisation of the clusters

4.1.1. PCA interpretation

The PCA1 made with time-integrated samples is similar to the one given by Sadaoui et al., (2016) with daily water discharge (**Figure 3a**). The F1 axis contains the information of water discharge variation for all tributaries while F2 axis separates the northern tributaries from the southern tributaries that have contrasted hydrologies in accordance with Pont et al., (2002). In PCA 2, F3 axis explains the temporal variability (spring vs autumn) and opposes alpine tributary hydrology to other hydrologies (**Figure 3b**).

4.1.2. Cluster hydrodynamic characterisation

Despite the use of integrated samples (and associated hydrological data) in this study that may aggregate several hydrological events, the five clusters defined are similar to the hydrological classification of the Rhône River made from daily water discharge (Pont et al., 2002, Sadaoui et al., 2016).

Cluster 1 is linked to southern tributary vectors (**Figure 3a**) and gathers southern flash-flood events (Pont et al., 2012, Eyrolle et al., 2012, Delile et al., 2020). No distinction between Cevenol and Mediterranean floods are proposed by the algorithm. The high standard deviations of average Q_{mean} and $C_{SPM\text{-}mean}$ highlight sharp variabilities. In the literature, southern events contribute the most on large export of SPM at the Rhône River scale. Eyrolle

et al., (2012) or Copard et al., (2018) demonstrated that, the Durance River could contribute to sediment load from < 1% to 80% during Mediterranean flood events. However, numerous studies have also estimated sediment budgets using geochemical methods and agree on the exceptional but non-negligible contribution of the Cevenol floods, that could occasionally reach more than 40% (Ollivier et al., 2011; Radakovitch et al., 2008; Zebracki et al., 2015).

Cluster 2 gathers oceanic regime with Q_{mean} distribution at Arles occurring during winter and the activation of the Saône and Upper Rhône rivers. The contrast between average $C_{SPM\text{-}mean}$ and Q_{mean} is explained by the main roles of these two tributaries as water suppliers. At the interannual scale, their contribution on water fluxes reaches more than 60% while their contribution in term of SPM (11 and 6 % respectively) are lower (Delile et al., 2020; Poulier et al., 2019; Sadaoui et al., 2016).

Cluster 3 observations occur during the end of spring season (**Figure 4**) and gather nival flood regime with net predominance of alpine rivers (Isère and Durance rivers) (**Figure 3b**). Their contribution can exceed 80 % in water fluxes and over 100% in SPM fluxes (Delile et al., 2020, Poulier et al., 2019).

Cluster 4 observations gather low-water level, during summer (**Figure 4**), with lowest Q_{mean} and $C_{SPM\text{-}mean}$. During such period, the production of autochthonous organic matter is increased as observed with the increase of %POC and %Chl.a (**Figure 4**).

Cluster 5, located at the center of the PCA1 (**Figure 3.a.**), gathers baseflow regime with medium Q_{mean} and $C_{SPM\text{-}mean}$ values. It occurs over spring and summer seasons (**Figure 4**) and the slight increases of Q_{mean} and $C_{SPM\text{-}mean}$ in the Durance and Isère rivers indicate nival episodes that might happen during these periods. As for Cluster 4, high values of %POC and %Chl.a indicate a production of autochthonous POC.

4.2. Classification of Δ^{14}C-POC

The Δ^{14}C-POC depletion observed for clusters 1 and 3 confirms the main knowledge presented in the literature about ^{14}C dynamic in the Rhône (Copard et al., 2018, Eyrolle et al., 2018; Eyrolle et al., in review). Indeed, the increase of $C_{SPM\text{-}mean}$ and the decrease of %POC (**Figure 7**) confirm the organic matter dilution with particulate mineral fractions by the weathering of carbonate rocks (Higueras et al., 2014). Then, rocks such as i) Black Marls, composed bare Mesozoic Badlands located among the French alps arc (Graz et al., 2011) or ii) Coal mines observed in slag heaps of Cevennes or mining operation sites in Briançonnais area of Alps, containing high contents of organic matter old of up 50 000 years BP. Because they are characterized by low vegetation density and violent hydroclimatic conditions, they could be considered as main sediment hotspots and could release consequent amount of organic matter (Eyrolle et al., in review). However, their contribution in sediment budget at the Rhône scale still poorly documented, excepted for the Durance River (Copard et al., 2018). Another source of such ^{14}C-depleted material might be the remobilisation of aging sediment POC trapped in flood plain across the main network (e.g., Leithold et al., 2016).

The case of Cluster 2 is different as the oceanic floods (Saône and Upper Rhône rivers) are characterized by a low level of $C_{SPM\text{-}mean}$. The range of Δ^{14}C-POC values and their disparity around 0 (**Figure 5**) can be explained by the fact that the SPM sampled for the measurement of Δ^{14}C-POC do not specifically come from these two tributaries. Since the samples are integrated over a period of about one month, they are very sensitive to floods that generate a lot of material or to anthropogenic inputs (e.g., dam flushing).

Cluster 4 and Cluster 5 present more enriched Δ^{14}C-POC (**Figure 5**), displaying a privileged autochthonous origin, related to high %Chl.a, for positive signatures (after 1950) showing

aquatic plants development preferentially higher when water flow and turbidity are low (**Figure 7**) (Higueras et al., 2014). High tritium concentrations, combined to high Δ^{14}C-POC values in clusters 4 and 5 might be related to the releases from the nuclear facilities (**Figure 7**). At the outlet of the Rhône River, the possibility of nuclear release increasing Δ^{14}C-POC is significant when %Chl.a is high suggesting a contamination of POC when primary productivity is important. Several studies have highlighted that ^{14}C is released as dissolved inorganic forms (DIC) because of oxidation processes applied in effluents before releases (e.g., Kang et al., 2019) and it could integrate POC through photosynthesis. However additional investigations might be conducted as the sampling methods were not the same for these two parameters and could lead to bias in the interpretation.

4.3. Relevance of Cluster analyses for classification of Δ^{14}C-POC signatures.

Figure 6 displays the complexity of hydrological classification of time-integrated sampling as a few samples are characterized by a mixture of clusters including several hydrological events and Δ^{14}C-POC signatures including different origins. Moreover, for the outliers (**Figure 5**), the relationship between the cluster classification and the Δ^{14}C-POC values is complex to explain and requires looking at the hydrograph during the sampling periods. For example, southern quick flood events have been registered in samples of low-water level related clusters (4 and 5) with depleted values of Δ^{14}C-POC. For Cluster 1, the positive value of Δ^{14}C-POC is observed in a sample with a southern flash flood occurring at the beginning of the sampling period but followed by a low-water level period favourable of Δ^{14}C-artificial POC. Cluster 1 samples also have consequent appurtenances to clusters 2 and 3. The sum of the membership degrees for the flood-related clusters (1, 2 and 3) is always higher than 58% and highlights that i) northern floods could also simultaneously occur than southern floods in autumn and ii) some southern floods could be observed during spring season as the same

484 time than nival flood events (**Figure 4**). The complex relationship of Cluster 2 with Δ^{14}C-POC
485 values is due to the low C_{SPM} load of the Saône and Upper Rhône river floods and the
486 consequent sensitivity to other events such as the Durance river floods or industrial
487 discharges. The main solution to reduce the disparity of the values would have been to use
488 the flux of SPM instead of the water discharge as the input data to determine the clusters.
489 Therefore, this would improve the classification of Δ^{14}C-POC values measured on SPM.
490 Unfortunately, such data was not available from all the tributaries and for the entire period
491 of study (starting since 2011), while clustering using water discharge was already commonly
492 used (Delaval et al., 2021). Finally, samples in the Cluster 5 seem to be a mix between the
493 Cluster 4 (low-water level cluster) and the flood-related clusters (1, 2 and 3). For this cluster,
494 centred in the PCA (**Figure 3**), the absence of relationship with the Δ^{14}C-POC values is directly
495 related to the complexity to categorize samples collected during baseflow.

496 ## 5. Conclusion

497 This study presents a first classification of time-integrated samples by clustering approach
498 according to the Rhône hydrology. Principal Component Analysis (PCA) followed by fuzzy-C
499 mean Cluster Analysis have been performed using time average of Q among the five major
500 water tributaries and the Upper Rhône River monitored at Jons. We used Δ^{14}C-POC data
501 collected in Particle Traps (PT) over a two-week to one-month sampling period as a
502 candidate to validate the classification. The classification exhibited 5 groups of hydrology
503 similar to that described in the literature: southern floods with Mediterranean and Cevenol
504 hydrologies confounded (Cluster 1), northern oceanic pluvial floods (Cluster 2), nival floods
505 (Cluster 3), but also baseflows (Cluster 5) and low-water levels (Cluster 4). Overall, Δ^{14}C-POC
506 distribution in time-integrated sample confirms the clustering classification according to

flood-related, baseflow and low-water level clusters. High Δ^{14}C-POC signatures, correlated to high tritium concentrations, are observed in clusters 4 and 5, incorporating nuclear releases, and are opposed against depleted signatures occurring during flood events observed in clusters 1 and 3 because of the Δ^{14}C-depleted material mobilisation from tributaries (e.g., black marls). The Δ^{14}C-POC outliers observed at each cluster show the sensitivity of PT samples to short events remobilising high sedimentary material or nuclear releases during a long sampling period especially for clusters 2 and 4. Furthermore, the overlaps of different events making difficult the Cluster Analysis to attribute the origins of Δ^{14}C-POC especially for flood clusters. Indeed, homogenous distribution of membership scores at some samples in clusters 1 to 3 shows a mixture of contrasted flood events over the sampling period. Because Cluster 5 is a mix of flood and low-water level events, some Δ^{14}C-POC values are incorrectly attributed here. If this method of classification with Q_{mean} showed pertinent results for Δ^{14}C-POC, applying SPM fluxes would improve the CA abilities to classify Δ^{14}C-POC according to the Rhône River hydrology. For this purpose, other signatures are expected for the coming years.

6. Acknowledgements

This study was supported by l'Observatoire des Sédiments du Rhône (OSR), a multi-partner research program funded by European Development Fund (Feder) and the Plan Rhône. ^{14}C and δ^{13}C analyses were carried out by le Laboratoire des Sciences du Climat et de l'Environnement (LSCE), le Laboratoire de Mesure du Carbone 14 (LMC14) (Saclay, France), and the MOOSE programm (https://www.moose-network.fr/fr/). We strongly thank the INRAE colleagues for providing the data. We are grateful to our IRSN colleagues, Franck Giner and David Mourier who managed the SPM sampling at Arles and southern OSR

stations. We also thank LSCE/LMC14 lab. colleagues, Jean-Pascal Dumoulin, Ingrid Caffy, Marc Sieudat, Emmanuelle Delque-Kolic and Christophe Moreau for the sample storage, preparation, graphitization and ^{14}C measurement.

References

AFNOR, 2005. NF EN 872 : Water Quality - Determination of suspended solids - Method by filtration through glass fibre filters. 14 (In French). pp.10.

Bezdek, J.C., Ehrlich, R., Full, W., 1984. FCM: The fuzzy c-means clustering algorithm. Comput. Geosci. 10 (2-3), 191–203. https://doi.org/10.1016/0098-3004(84)90020-7

Chaimontree, S., Atkinson, K., Coenen, F., 2010. Best Clustering Configuration Metrics: Towards Multiagent Based Clustering, in Advanced data mining and applications Part 1, Springer (2010), pp. 48-60.

Copard, Y., Eyrolle, F., Radakovitch, O., Poirel, A., Raimbault, P., Gairoard, S., Di-Giovanni, C., 2018. Badlands as a hot spot of petrogenic contribution to riverine particulate organic carbon to the Gulf of Lion (NW Mediterranean Sea). Earth Surf. Process. Landforms 43, 2495–2509. https://doi.org/10.1002/esp.4409

Cottereau, E., Arnold, M., Moreau, C., Baqué, D., Bavay, D., Caffy, I., Comby, C., Dumoulin, J.P., Hain, S., Perron, M., Salomon, J., Setti, V., 2007. Artemis, the new 14C AMS at LMC14 in Saclay, France. Radiocarbon 49, 291–299. https://doi.org/10.1017/S0033822200042211

Delaval, A., Duffa, C., Pairaud, I., Radakovitch, O., 2021. A fuzzy classification of the hydrodynamic forcings of the Rhone River plume: An application in case of accidental

552 release of radionuclides. Environ. Model. Softw. 140, 105005.
553 https://doi.org/10.1016/j.envsoft.2021.105005

554 Delile, H., Masson, M., Miège, C., Le Coz, J., Poulier, G., Le Bescond, C., Radakovitch, O.,
555 Coquery, M., 2020. Hydro-climatic drivers of land-based organic and inorganic
556 particulate micropollutant fluxes: The regime of the largest river water inflow of the
557 Mediterranean Sea. Water Res. 185, 116067.
558 https://doi.org/10.1016/j.watres.2020.116067

559 Ducros, L., 2018. Origine et devenir du tritium au sein des hydrosystèmes continentaux
560 méditerranéens français. (Doctoral dissertation). Aix-Marseille Univsersity, Marseille,
561 France.

562 Dumoulin, J.P., Comby-Zerbino, C., Delqué-Količ, E., Moreau, C., Caffy, I., Hain, S., Perron, M.,
563 Thellier, B., Setti, V., Berthier, B., Beck, L., 2017. Status Report on Sample Preparation
564 Protocols Developed at the LMC14 Laboratory, Saclay, France: From Sample Collection
565 to 14C AMS Measurement. Radiocarbon 59, 713–726.
566 https://doi.org/10.1017/RDC.2016.116

567 Eyrolle, F., Lepage, H., Antonelli, C., Morereau, A., Cossonnet, C., Boyer, P., Gurriaran, R.,
568 2020. Radionuclides in waters and suspended sediments in the Rhone River (France) -
569 Current contents, anthropic pressures and trajectories. Sci. Total Environ. 723.
570 https://doi.org/10.1016/j.scitotenv.2020.137873

571 Eyrolle, F., Lepage, H., Copard, Y., Ducros, L., Claval, D., Saey, L., Cossonnet, C., Giner, F.,
572 Mourier, D., 2018. A brief history of origins and contents of Organically Bound Tritium
573 (OBT) and 14C in the sediments of the Rhône watershed. Sci. Total Environ. 643, 40–51.
574 https://doi.org/10.1016/j.scitotenv.2018.06.074

575 Eyrolle, F., Radakovitch, O., Copard, Y., Lepage, H., Bodereau, N., Raimbault, P., Dabrin, A.,
576 Lagadec, V., Le Corre, C., n.d. Tritium and 14C dependencies upon Particulate Organic
577 Matter within the nuclearized Rhone River (France). Journal of Soil and Sediment, in
578 review.

579 Ferraro, M.B., Giordani, P., Serafini, A., 2019. Fclust: An R package for fuzzy clustering. R J.
580 11, 1–18. https://doi.org/10.32614/rj-2019-017

581 Godwin, H., Willis, E.H., Hill, S., 1962. Natural Radiocarbon Measurements V. Radiocarbon 4,
582 57–70.

583 Graz, Y., Di-Giovanni, C., Copard, Y., Elie, M., Faure, P., Laggoun Defarge, F., Lévèque, J.,
584 Michels, R., Olivier, J.E., 2011. Occurrence of fossil organic matter in modern
585 environments: Optical, geochemical and isotopic evidence. Appl. Geochemistry 26,
586 1302–1314. https://doi.org/10.1016/j.apgeochem.2011.05.004

587 Hannah, D.M., Smith, B.P.G., Gurnell, A.M., McGregor, G.R., 2000. An approach to
588 hydrograph classification. Hydrol. Process. 14, 317–338.
589 https://doi.org/10.1002/(SICI)1099-1085(20000215)14:2<317::AID-HYP929>3.0.CO;2-T

590 Higueras, M., Kerhervé, P., Sanchez-Vidal, A., Calafat, A., Ludwig, W., Verdoit-Jarraya, M.,
591 Heussner, S., Canals, M., 2014. Biogeochemical characterization of the riverine
592 particulate organic matter transferred to the NW Mediterranean Sea. Biogeosciences
593 11, 157–172. https://doi.org/10.5194/bg-11-157-2014

594 Horowitz, A.J., Elrick, K.A., Smith, J.J., 2001. Estimating suspended sediment and trace
595 element fluxes in large river basins: Methodological considerations as applied to the
596 NASQAN programme. Hydrol. Process. 15, 1107–1132. https://doi.org/10.1002/hyp.206

597 Husson, F., Josse, J., Pagès, J., 2010. L'analyse de données avec R - Complémentarité des
598 Méthodes d'analyse factorielle et de classification. 42èmes Journées de Statistique,
599 2010, Marseille, France, France. inria-00494779

600 Jain, A.K., Murty, M.N., Flynn, P.J., 1999. Data clustering: A review. ACM Comput. Surv. 31,
601 264–323. https://doi.org/10.1145/331499.331504

602 Javed, A., Hamshaw, S.D., Lee, B.S., Rizzo, D.M., 2021. Multivariate event time series analysis
603 using hydrological and suspended sediment data. J. Hydrol. 593, 125802.
604 https://doi.org/10.1016/j.jhydrol.2020.125802

605 Jean-Baptiste, P., Fontugne, M., Fourré, E., Marang, L., Antonelli, C., Charmasson, S., Siclet,
606 F., 2018. Tritium and radiocarbon levels in the Rhône river delta and along the French
607 Mediterranean coastline. J. Environ. Radioact. 187, 53–64.
608 https://doi.org/10.1016/j.jenvrad.2018.01.031

609 Kamel, M., Selim, S., 1994. New Algorithms for Solving the Fuzzy Clustering Problem. Pattern
610 Recognit. 27, 421–428.

611 Kang, D., Lee, J., Kim, S., Noh, S., & Kang, S. (2019). Evaluation on ^{14}C emission patterns of
612 various PWR types in South Korea and effectiveness of inventory reduction driving
613 (IRD). *Journal of Radioanalytical and Nuclear Chemistry*, 322(3), 1409–1415.
614 https://doi.org/10.1007/s10967-019-06805-1

615 Kim, H.S., Kim, J.H., Ho, C.H., Chu, P.S., 2011. Pattern classification of typhoon tracks using
616 the fuzzy c-means clustering method. J. Clim. 24, 488–508.
617 https://doi.org/10.1175/2010JCLI3751.1

618 Klawonn, F., Höppner, F., 2003. What Is Fuzzy about Fuzzy Clustering? Understanding and

619 Improving the Concept of the Fuzzifier, in: Advances in Intelligent Data Analysis V. pp.
620 254–264.

621 Launay, M., Dugué, V., Faure, J.B., Coquery, M., Camenen, B., Le Coz, J., 2019. Numerical
622 modelling of the suspended particulate matter dynamics in a regulated river network.
623 Sci. Total Environ. 665, 591–605. https://doi.org/10.1016/j.scitotenv.2019.02.015

624

625 Lepage, H., Gruat, A., Thollet, F., Le Coz, J., Coquery, M., Masson, M., Dabrin, A.,
626 Radakovitch, O., Eyrolle, F., Labille, J., Ambrosi, J.-P., Delanghe, D., Raimbault, P., 2022.
627 Concentrations and fluxes of suspended particulate matters and associated
628 contaminants in the Rhône River from Lake Geneva to the Mediterranean Sea. Earth
629 Syst. Sci. Data 7, 1–22. https://doi.org/10.5194/essd-2021-350

630

631 Leithold, E.L., Blair, N.E., Wegmann, K.W., 2016. Source-to-sink sedimentary systems and
632 global carbon burial: A river runs through it. Earth-Science Rev. 153, 30–42.
633 https://doi.org/10.1016/j.earscirev.2015.10.011

634 Masson, M., Angot, H., Le Bescond, C., Launay, M., Dabrin, A., Miège, C., Le Coz, J., Coquery,
635 M., 2018. Sampling of suspended particulate matter using particle traps in the Rhône
636 River: Relevance and representativeness for the monitoring of contaminants. Sci. Total
637 Environ. 637–638, 538–549. https://doi.org/10.1016/j.scitotenv.2018.04.343

638 Meybeck, M., 2003. Global analysis of river systems: From Earth system controls to
639 Anthropocene syndromes. Philos. Trans. R. Soc. B Biol. Sci. 358, 1935–1955.
640 https://doi.org/10.1098/rstb.2003.1379

641 Meybeck, M., 1982. Carbon, nitrogen, and phosphorus transport by world rivers. Am. J. Sci.
642 https://doi.org/10.2475/ajs.282.4.401

643 Meyer, D., Dimitriadou, E., Hornik, K., Weingessel, A., Leisch, F., Chang, C.-C., Lin, C.-C., 2021.
644 Package 'e1071' : Misc Functions of the Department of Statistics, Probability Theory
645 Group (Formerly: E1071), TU Wien Imports.

646 Milliman, J.D., Farnsworth, K.L., 2011. River discharge to the coastal ocean: A global
647 synthesis, River Discharge to the Coastal Ocean: A Global Synthesis.
648 https://doi.org/10.1017/CBO9780511781247

649 Misset, C., Recking, A., Legout, C., Valsangkar, N., Bodereau, N., Zanker, S., Poirel, A.,
650 Borgniet, L., 2019. The Dynamics of Suspended Sediment in a Typical Alpine Alluvial
651 River Reach: Insight From a Seasonal Survey. Water Resour. Res. 55, 10918–10934.
652 https://doi.org/10.1029/2019WR025222

653 Mourier, B., Desmet, M., Van Metre, P.C., Mahler, B.J., Perrodin, Y., Roux, G., Bedell, J.P.,
654 Lefèvre, I., Babut, M., 2014. Historical records, sources, and spatial trends of PCBs along
655 the Rhône River (France). Sci. Total Environ. 476–477, 568–576.
656 https://doi.org/10.1016/j.scitotenv.2014.01.026

657 Olivier, J.M., Carrel, G., Lamouroux, N., Dole-Olivier, M.J., Malard, F., Bravard, J.P., Amoros,
658 C., 2009. The Rhône River Basin, Rivers of Europe. https://doi.org/10.1016/B978-0-12-
659 369449-2.00007-2

660 Ollivier, P., Radakovitch, O., Hamelin, B., 2011. Major and trace element partition and fluxes
661 in the Rhône River. Chem. Geol. 285, 15–31.
662 https://doi.org/10.1016/j.chemgeo.2011.02.011

663 Ouyang, R., Ren, L., Cheng, W., Zhou, C., 2010. Similarity search and pattern discovery in
664 hydrological time series data mining. Hydrol. Process. 24, 1198–1210.
665 https://doi.org/10.1002/hyp.7583

666 Phillips, J.M., Russell, M.A., Walling, D.E., 2000. Time-integrated sampling of fluvial
667 suspended sediment: A simple methodology for small catchments. Hydrol. Process. 14,
668 2589–2602. https://doi.org/10.1002/1099-1085(20001015)14:14<2589::AID-
669 HYP94>3.0.CO;2-D

670 Pont, D., Simonnet, J.-P., Walter, A.V., 2002. Medium-term Changes in Suspended Sediment
671 Delivery to the Ocean: Consequences of Catchment Heterogeneity and River
672 Management (Rhône River, France). Estuar. Coast. Shelf Sci. 54, 1–18.
673 https://doi.org/10.1006/ecss.2001.0829

674 Poulier, G., Launay, M., Le Bescond, C., Thollet, F., Coquery, M., Le Coz, J., 2019. Combining
675 flux monitoring and data reconstruction to establish annual budgets of suspended
676 particulate matter, mercury and PCB in the Rhône River from Lake Geneva to the
677 Mediterranean Sea. Sci. Total Environ. 658, 457–473.
678 https://doi.org/10.1016/j.scitotenv.2018.12.075

679 Radakovitch, O., Roussiez, V., Ollivier, P., Ludwig, W., Grenz, C., Probst, J.L., 2008. Input of
680 particulate heavy metals from rivers and associated sedimentary deposits on the Gulf of
681 Lion continental shelf. Estuar. Coast. Shelf Sci. 77, 285–295.
682 https://doi.org/10.1016/j.ecss.2007.09.028

683 Raimbault P., Neveux J., Lantoine F., 2004. Dosage rapide de la chlorophylle a et des
684 phaeopigments a par fluorimétrie après extraction au méthanol. Comparaison avec la
685 méthode classique d'extraction à l'acétone. Oceanis, 30(2) : 189-205.

686 Raimbault, P., Garcia, N., Cerutti, F., 2008. Distribution of inorganic and organic nutrients in
687 the South Pacific Ocean – evidence for long-term accumulation of organic matter in
688 nitrogen-depleted waters. Biogeosciences 5, 281–298. https://doi.org/10.5194/bg-5-
689 281-2008

690 Ramze Rezaee, M., Lelieveldt, B.P.F., Reiber, J.H.C., 1998. A new cluster validity index for the
691 fuzzy c-mean. Pattern Recognit. Lett. 19, 237–246. https://doi.org/10.1016/S0167-
692 8655(97)00168-2

693 Raux, J., Copard, Y., Laignel, B., Fournier, M., Masseï, N., 2011. Classification of worldwide
694 drainage basins through the multivariate analysis of variables controlling their
695 hydrosedimentary response. Glob. Planet. Change 76, 117–127.
696 https://doi.org/10.1016/j.gloplacha.2010.12.005

697 Raymond, P.A., Bauer, J.E., 2001. Use of 14C and 13C natural abundances for evaluating
698 riverine, estuarine, and coastal DOC and POC sources and cycling: A review and
699 synthesis. Org. Geochem. 32, 469–485. https://doi.org/10.1016/S0146-6380(00)00190-
700 X

701 Sadaoui, M., Ludwig, W., Bourrin, F., Raimbault, P., 2016. Controls, budgets and varaiability
702 of riverine sediment fluxes to the Gulf of Lions (NW Mediterranean Sea). J. Hydrol. 540,
703 1002–1015. https://doi.org/10.1016/j.jhydrol.2016.07.012

704 Schulze, T., Ricking, M., Schröter-Kermani, C., Körner, A., Denner, H.-D., Weinfurtner, K.,
705 Winkler, A., Pekdeger, A., 2007. The German Environmental Specimen Bank - Sampling,
706 processing, and archiving sediment and suspended particulate matter. J. Soils
707 Sediments 7, 361–367. https://doi.org/10.1065/jss2007.08.248

Schwämmle, V., Jensen, O.N., 2010. A simple and fast method to determine the parameters for fuzzy c-means cluster analysis. Bioinformatics 26, 2841–2848. https://doi.org/10.1093/bioinformatics/btq534

Stuiver, M., Polach, H.-A., 1977. Reporting of 14C data. Radiocarbon 19(3), 355-363. https://doi.org/10.1017/S0033822200003672

Thollet, F., Le Bescond, C., Lagouy, M., Gruat A., Grisot, G., Le Coz, J., Coquery, M., Lepage, H., Gairoard, S., Gattacceca, J.C., Ambrosi, J.-P., Radakovitch, O., Dur, G., Richard, L., Giner, F., Eyrolle, F., Angot, H., Mourier, D., Bonnefoy, A., Dugué, V., Launay, M., Troudet, L., Labille, J., Kieffer, L. (2021): Développement de l'application informatique BDOH pour l'Observatoire des Sédiments du Rhône [Research report] INRAE. 2021. https://dx.doi.org/10.17180/OBS.OSR

Trumbore, S.E., Sierra, C.A., Hick Pries, C.E., 2016. Radiocarbon Nomenclature, Theory, Models, and Interpretation : Measuring Age,determining cycling rates, and Tracing Source Roles, in: Schuur, E.A.G., Druffel, E.R.M., Trumbore, S.E. (Eds.), Radiocarbon and Climate Change, Mechanisms, Applications and Laboratory Techniques. Springer International Publishing, pp. 45–82.

Voegel, J.S., Southon, J.R., Nelson, D.E., Brown, T.A., 1984. Performance of catalytically condensed carbon for use in Accelerator Mass Spectrometry. Nucl. Instruments Methods Phys. Res. 5, 289–293.

Walling, D.E., Owens, P.N., Carter, J., Leeks, G.J.L., Lewis, S., Meharg, A.A., Wright, J., 2003. Storage of sediment-associated nutrients and contaminants in river channel and

floodplain systems. Appl. Geochemistry 18, 195–220. https://doi.org/10.1016/S0883-2927(02)00121-X

Zebracki, M., Eyrolle-Boyer, F., Evrard, O., Claval, D., Mourier, D., Gairoard, S., Cagnat, X., Antonelli, C., 2015. Tracing the origin of suspended sediment in a large Mediterranean river by combining continuous river monitoring and measurment of artificial and natural radionuclides. Sci. Total Environ. 502, 122–213.

750